Design of photonic metamaterial multi-junction solar cells using rigorous coupled wave analysis

Eli Lansey[a] and David T. Crouse[b]

[a]Department of Physics
[b]Department of Electrical Engineering
The City College of New York, New York, NY, USA 10031

August 26, 2010

ABSTRACT

We have developed a method to design multi-junction horizontally-oriented solar cells using single-layer photonic metamaterials. These metamaterial light harvesting templates are capable of separating white light into discrete wavelength ranges and trapping it efficiently into different, separately wired cavities. Any number of different wavelength-tailored charge separation complexes can be fixed to the walls of these tuned cavities. To design the metamaterials we have developed a coupled wave analysis of 2D periodic metamaterials. Past results with 1D gratings have shown that this is a very effective method for designing periodic structures and we have generalized the approach to 2D periodic cavities.

Keywords: Metamaterial, multijunction solar cell, coupled wave analysis, cavity mode, light harvesting, opto-electronic devices

1. INTRODUCTION

Anomalous optical transmission (AOT) through subwavelength apertures was first observed by T.W. Ebbesen in 1998 and described in his article in *Nature* on optical characteristics of metallic thin films perforated with subwavelength-sized apertures, an article that launched the field of research focused on metamaterials and anomalous transmission.[1] Ebbesen described transmission of light through apertures with diameters significantly smaller than the wavelength of light being studied, a phenomenon thought impossible under the paradigm of aperture theory.[2,3]

Research into metamaterials (also called plasmonic crystals) has advanced greatly since 1998, with many novel and useful optical phenomena observed in these structures, including: negative index of refraction,[4] light concentration and trapping,[5] and light distribution/beam splitting.[6] Metamaterials can also increase the performance of renewable ("green") energy devices by selectively channeling and filtering light of different wavelengths into separate subwavelength apertures or cavities.

One of us (D.T.C) has shown the effectiveness of light channeling and trapping produced by cavity modes (CMs). He has found, both theoretically/numerically and experimentally,[7–9] that CM-produced light trapping can lead to exceptionally high light amplifications within the confined spaces of 1D cavities (gratings), allowing charge-separation domains to be bathed in a constant supply of photons, even under low light conditions. In this paper we describe a method of designing a horizontally-oriented multi-junction solar cell by creating an array of cavities tuned with targeted CMs.

To design the metamaterials we have developed a coupled wave analysis of 2D periodic metamaterials. Past results with 1D gratings have shown that this is a very effective method for designing periodic structures and we have generalized the approach to 2D periodic cavities. In this paper we always assume an implicit $e^{-i\omega t}$ time dependance. Additionally, unless specially noted, we use CGS units throughout this paper.

Further author information: (Send correspondence to E.L)
E.L.: E-mail: elansey@gc.cuny.edu, Telephone: 1 212 650 7415
D.T.C.: E-mail: dcrouse@ccny.cuny.edu, Telephone: 1 212 650 7280

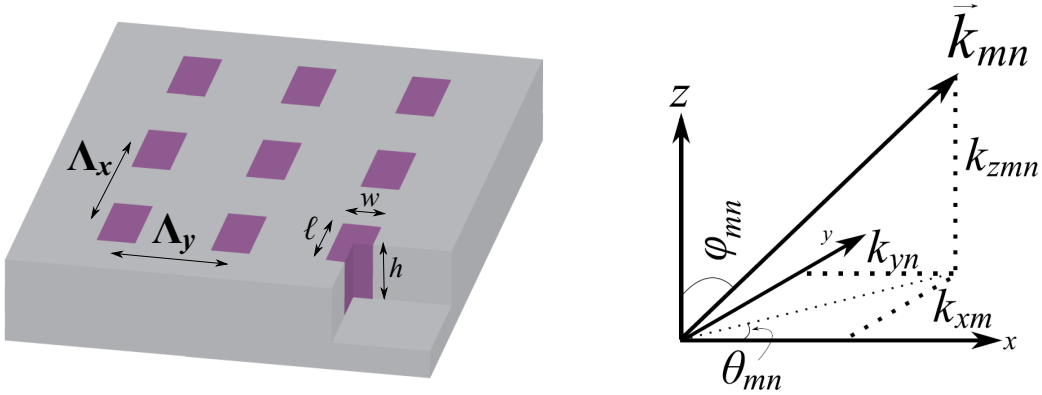

(a) Overall geometry of the system.

(b) Geometry of Floquet mode wave vectors.

Figure 1. Geometry of the system and wave vectors.

The system we are modeling consists of a thin metallic film, perforated with a 2D array of rectangular cavities with rectangularly periodic spacing. That is, if a template cavity is centered at the origin, the positions of the centers of all the other cavities $\vec{c}$ are given by

$$\vec{c} = m\Lambda_x\hat{x} + n\Lambda_y\hat{y} \tag{1}$$

where m, n are integers, and Λ_x and Λ_y are the lattice spacings in the x and y directions directions, respectively. See Fig. 1(a).

This system is broken into three vertical layers: superstrate, metallic substrate and perforated cavity regions of the film. We will expand both the electric and magnetic fields in terms of sets of basis functions appropriate for each region. Namely, in the superstrate, where we expect the overall field to behave largely like plane waves, we expand in terms of a basis set of plane waves satisfying the Floquet mode condition to be described in Section 3. In the cavities, however, it is more natural to expand the field in terms of waveguide cavity modes. That is, for rectangular cavities, the set of cavity modes will include be sine and cosine functions. This will be discussed in Section 4.

2. SOLUTION STRATEGY

Our solution strategy, at the most basic level, is simply to apply electromagnetic boundary conditions at the interfaces of the the metallic film and require continuity of the fields across the cavity interface. Furthermore, it's useful to decompose an arbitrary electromagnetic field into two orthogonal polarizations. Then applying these conditions, multiplying by orthogonal basis functions and integrating over the interfaces will eventually yield a set of equations for the field expansion coefficients.

2.1 Polarization schemes

Waveguide fields are usually broken down into TM ($B_z = 0$) and TE ($E_z = 0$) polarizations. In general, TEM ($B_z = 0$ and $E_z = 0$) cavity polarizations can also exist, but for cavities of a single surface of reasonably high conductivity these modes are non-existent. For coaxial and grating-type structures, and for lossy metals, however, TEM modes must be included. These cavity polarizations are completely orthogonal; transverse fields for each polarization are uniquely specified by the z-components of the field. Therefore, any arbitrary field within the cavities with both E_z and B_z components can be split into TM and TE parts, and once E_z and B_z are known, the remaining field components for each polarization can be calculated separately and independently of the other.

We will likewise separate the fields in the superstrate into these two polarizations. Then, an incident plane wave with TM polarization in the superstrate, for example, has a E_z component while $B_z = 0$. Continuity of the

E and B fields across the cavity interface ensures that the only cavity modes that can *directly* couple with this incident TM plane wave are ones with $B_z = 0$, namely cavity TM modes. Then, the TE cavity modes, likewise, will only directly interact with an incident plane wave with TE polarizations where $E_z = 0$.

However, scattered fields produced by this TM incident wave can, in general, have B_z components. But, in order to satisfy the condition that the net $B_z = 0$, for a given scattered field with $B_z \neq 0$, there must be other fields with equal and opposite B_z components. This leaves us, though, with the existence of scattered or diffracted fields of both polarizations for an incident beam having a single polarization, and thus an incident TM wave can, *indirectly*, couple to TE cavity modes through scattered fields.

As an illustrative example, we'll consider a normally-incident plane wave. In our language, this beam has a TEM polarization; both E and B must be perpendicular to the $\vec{k} = k\hat{z}$ vector thus, there is neither a B_z nor an E_z component to the fields. In practice, what this implies is that the incident beam can not *directly* couple to *any* cavity modes. However, scattered fields can have both B_z and E_z, and thus even a TEM beam can couple to both TM and TE polarizations. Thus, it is through scattering that coupling between TE and TM modes arises, even for non-normal incident waves.

2.2 Boundary conditions

In order to solve our problem, we use different boundary conditions at different types of interfaces: Continuity of fields across cavity-superstrate or cavity-substrate interfaces, so-called "surface impedance boundary conditions" (SIBC) at metal-superstrate interfaces and a skin-depth approximation boundary condition (SDBC) at cavity walls.

We require that the electric and magnetic fields remain continuous across the cavity-superstrate (and cavity-substrate interfaces for open channels), as mentioned earlier. From Jackson,[10] from Maxwell's equations, we have continuity of the electric displacement vector

$$\epsilon_1 \vec{E}_1, = \epsilon_2 \vec{E}_2, \tag{2}$$

across a boundary between two regions 1 and 2. Similarly,

$$\vec{H}_2 = \vec{H}_1 \tag{3}$$

the magnetic field must be continuous (we assume $\mu_1 = \mu_2 = 1$) across the boundary, as well.

At metallic interfaces we have a choice of a few conditions. The simplest is that of a perfect conductor where

$$\hat{n} \times \vec{E} = 0 \tag{4a}$$

$$\hat{n} \cdot \vec{H} = 0 \tag{4b}$$

evaluated at the surface, where $\hat{n}$ is the unit normal to the surface.[10]

In a good conductor, however, the field does not stop immediately upon entering the metal. Instead, the magnitude of the fields decay exponentially with a characteristic length

$$\delta \approx \frac{c}{\sqrt{2\pi\omega\sigma}}, \tag{5}$$

where σ is the conductivity of the metal, and δ is the "skin depth" of the field. In MKSA δ is[10]

$$\delta \approx \sqrt{2/\omega\sigma}. \tag{6}$$

The skin depth is much smaller than any cavity dimension, and thus we expect the overall spacial dependance of the fields to be largely similar to those of a perfect conductor. In this skin depth approximation, we assume that at a depth greater than δ inside the metal, the field drops exponentially to zero so at that depth the metal effectively becomes a perfect conductor. Thus, we apply the perfect conductor boundary conditions Eqs. (4) at the skin depth, rather than at the metal surface.

We define

$$\zeta \equiv \frac{\delta}{\ell} \tag{7}$$

as the unitless ratio of skin depth to the characteristic cavity dimension ℓ. We want to estimate the value of ζ. To that end, only for this, we'll use MKSA units. We choose our ℓ using an infinite rectangular waveguide cutoff condition. For a lowest order mode we have $\omega = \pi/\sqrt{\epsilon}\ell$, or $\ell = \pi/\sqrt{\epsilon}\omega$. Then, using $\omega = 2\pi f$ and $\epsilon = \epsilon_r\epsilon_0$ and Eq. 6, $\zeta = \sqrt{4\epsilon_0\epsilon_r f/\pi\sigma}$.

For frequencies in Hz and conductivities in Siemens/meter $\zeta \sim 10^{-6}\sqrt{\epsilon_r f/\sigma}$. Metal conductivies are in the order 5×10^7 Siemens/meter. Thus, $\zeta \sim 10^{-10}\sqrt{\epsilon_r f}$. The largest dielectrics currently in use (semiconductors) have $\epsilon_r \sim 10$, so for the most extreme case, $\zeta \sim 10^{-9}\sqrt{f}$. Thus, ζ remains small ($\ll 1$) for frequencies approaching low-energy X-rays (10^{16} Hz). In the terahertz (visible) range, $\zeta \sim 10^{-3}$. This allows us to find relationships between field components and the resonances of the cavity.

The SIBC condition is an approximation which holds for good conductors.[11] The condition is

$$\vec{E}_{\|} = \mathcal{Z}\hat{n} \times \vec{H}_{\|}, \tag{8}$$

where $\mathcal{Z} = 1/n$ is the impedance of the metal, where n is the, in general complex, index of refraction of the metal, $E_{\|}$ and $H_{\|}$ are the electric and magnetic fields tangent to the interface and $\hat{n}$ is the unit normal out of the metal.

3. FLOQUET MODES

The waves in the superstrate satisfy the Floquet condition due to the periodicity of the lattice. The superstrate is filled with a nonmagnetic material ($\mu = 1$) and a dielectric ϵ_a.

The spacial dependance of Floquet modes traveling the in $\pm\hat{z}$ direction is

$$\exp[\vec{k}_{mn} \cdot \vec{r}] = \exp\left[i\left(k_{xm}x + k_{yn}y \pm k_{zmn}z\right)\right], \tag{9}$$

where the choice of sign before $k_{zmn}z$ is positive for upward propagating waves, and negative for downward propagating waves. Through the rest of these calculations, if we have a $\pm$ or $\mp$ we'll assume the upper symbol refers to upward propagating and the lower symbol to downward propagating waves.

If we define $\kappa_0 \equiv 2\pi/\lambda = \omega/c$, then the magnitude of the incident wavevector $k_0 = \sqrt{\epsilon_a}\kappa_0$, for non-magnetic material. Then, the Floquet conditions on k_{xm}, k_{yn} and k_{zmn} are

$$k_{xm} = k_{x0} + mK_x, \qquad k_{yn} = k_{y0} + nK_y, \qquad k_{zmn} = \xi_{mn}\sqrt{\epsilon_a}\kappa_0 \tag{10}$$

where m and n are integers, k_{x0} and k_{y0} are the x and y components of the incident wavevector, and K_x and K_y are the reciprocal lattice vectors. Here

$$k_{x0} = k_0 \sin\varphi_i \cos\theta_i, \qquad k_{y0} = k_0 \sin\varphi_i \sin\theta_i, \tag{11}$$

where φ_i is the inclination and θ_i is the azimuthal angle of the incoming wavevector, see Fig. 1(b), K_x and K_y are

$$K_x = \frac{2\pi}{\Lambda_x}, \qquad K_y = \frac{2\pi}{\Lambda_y}, \qquad \xi_{mn} \equiv \sqrt{1 - \frac{k_{xm}^2 + k_{yn}^2}{\epsilon_a\kappa_0^2}}, \tag{12}$$

where ξ_{mn} takes values between 0 and 1 depending, essentially, on what fraction of the total energy of the wave is traveling in the transverse direction.

3.1 Polarization Schemes

Now, for each $\vec{k}_{mn}$ there are two polarizations: One polarization has $H_z = 0$ (TM polarization) and the other has $E_z = 0$ (TE polarization). By application of Maxwell's equations, we can relate the magnitudes of the electric and magnetic fields for each polarization.[12]

For the TM polarization we choose

$$H_{zmn}^{TM} = 0. \tag{13}$$

Using conditions imposed by Maxwell's equations, we can write the magnitude of the z component of the electric field as

$$E_{zmn}^{TM} = \pm\frac{1}{\sqrt{\epsilon_a}}\sin\varphi_{mn} H_{mn}^{TM}. \tag{14}$$

Here our expansion coefficient is the magnitude of the magnetic field H_{mn}^{TM}.

For the TE Polarization we choose

$$E_{zmn}^{TE} = 0. \tag{15}$$

Using condition imposed by Maxwell's equations, we can write the magnitude of the z component of the magnetic field as

$$H_{zmn}^{TE} = \mp\sqrt{\epsilon}_a \sin\varphi_{mn} E_{mn}^{TE}. \tag{16}$$

Here our expansion coefficient is the magnitude of the magnetic field E_{mn}^{TE}.

3.2 Total Fields in the Superstrate

We can now write the total z components of electric and magnetic fields in the superstrate as the sum of all the individual TM and TE modes. As a notation convention, in the expressions for incident waves, we will replace the H_{mn}^{TM} expansion coefficients with I_{mn}^{TM} and the E_{mn}^{TE} expansion coefficients with I_{mn}^{TE}. Then,

$$\begin{aligned} H_x^{\text{super}} = &\sum_{m,n}\left(\sin\theta_{mn} I_{mn}^{TM} - \sqrt{\epsilon_a}\,\xi_{mn}\cos\theta_{mn} I_{mn}^{TE}\right) e^{i[k_{xm}x + k_{yn}y - k_{zmn}(z-h/2)]} \\ &+ \sum_{m,n}\left(\sin\theta_{mn} H_{mn}^{TM} + \sqrt{\epsilon_a}\,\xi_{mn}\cos\theta_{mn} E_{mn}^{TE}\right) e^{i[k_{xm}x + k_{yn}y + k_{zmn}(z-h/2)]} \end{aligned} \tag{17a}$$

$$\begin{aligned} H_y^{\text{super}} = &\sum_{m,n}\left(-\cos\theta_{mn} I_{mn}^{TM} - \sqrt{\epsilon}_a\,\xi_{mn}\sin\theta_{mn} I_{mn}^{TE}\right) e^{i[k_{xm}x + k_{yn}y - k_{zmn}(z-h/2)]} \\ &+ \sum_{m,n}\left(-\cos\theta_{mn} H_{mn}^{TM} + \sqrt{\epsilon}_a\,\xi_{mn}\sin\theta_{mn} E_{mn}^{TE}\right) e^{i[k_{xm}x + k_{yn}y + k_{zmn}(z-h/2)]} \end{aligned} \tag{17b}$$

$$\begin{aligned} E_x^{\text{super}} = &\sum_{m,n}\left(-\frac{1}{\sqrt{\epsilon}_a}\,\xi_{mn}\cos\theta_{mn} I_{mn}^{TM} + \sin\theta_{mn} I_{mn}^{TE}\right) e^{i[k_{xm}x + k_{yn}y - k_{zmn}(z-h/2)]} \\ &+ \sum_{m,n}\left(\frac{1}{\sqrt{\epsilon}_a}\,\xi_{mn}\cos\theta_{mn} H_{mn}^{TM} + \sin\theta_{mn} E_{mn}^{TE}\right) e^{i[k_{xm}x + k_{yn}y + k_{zmn}(z-h/2)]} \end{aligned} \tag{17c}$$

$$\begin{aligned} E_y^{\text{super}} = &\sum_{m,n}\left(-\frac{1}{\sqrt{\epsilon}_a}\,\xi_{mn}\sin\theta_{mn} I_{mn}^{TM} - \cos\theta_{mn} I_{mn}^{TE}\right) e^{i[k_{xm}x + k_{yn}y - k_{zmn}(z-h/2)]} \\ &+ \sum_{m,n}\left(\frac{1}{\sqrt{\epsilon}_a}\,\xi_{mn}\sin\theta_{mn} H_{mn}^{TM} - \cos\theta_{mn} E_{mn}^{TE}\right) e^{i[k_{xm}x + k_{yn}y + k_{zmn}(z-h/2)]} \end{aligned} \tag{17d}$$

4. RECTANGULAR CAVITY MODES

Here we consider a cavity filled with a dielectric ϵ_c, with edges $-\ell/2 \le x \le \ell/2$, $-w/2 \le y \le w/2$ and $-h/2 \le z \le h/2$, see Fig. 1(b). The normal fields F_z are

$$F_z(x,y) = \sum_{s,l} \psi_{sl}(x,y) e^{\pm i\gamma_{sl}(z+h/2)} \tag{18}$$

where F stands in place of E or H and where ψ_{sl} are solutions to the wave equation

$$\left[\nabla^2 + \left(\epsilon\kappa_0^2 - \gamma^2\right)\right] \psi_{sl} = 0 \tag{19}$$

with appropriate boundary conditions.

Solving the wave equation (Eq. 19) gives

$$\psi_{sl} = \mathcal{E}_{sl} \left\{ A \sin\left[\alpha_s\left(x - \frac{\ell}{2}\right)\right] + B\cos\left[\alpha_s\left(x-\frac{\ell}{2}\right)\right]\right\}\left\{C\sin\left[\beta_l\left(y-\frac{w}{2}\right)\right] + D\cos\left[\beta_l\left(y-\frac{w}{2}\right)\right]\right\}, \tag{20}$$

where $\gamma_{sl}^2 = \epsilon\kappa_0^2 - \alpha_s^2 - \beta_l^2$ and $\mathcal{E}_{sl} = \sqrt{4/\ell w}$ and where there are additional constraints on A, B, C, D and on the values of α_s and β_l depending on the boundary conditions (perfect conductor or skin-depth approximation). Furthermore, there is a relationship between A and B as well as between C and D which allows further simplification of this expression. See Appendix A for details. We will use the results in Appendix A to choose which of these coefficients (A, B, C, D) to eliminate, allowing us to write $\psi_{sl} = \mathcal{E}_{sl}\mathcal{G}_{sl} \times U(x,y)$, where, $\mathcal{G}_{sl}$ is the expansion coefficient for the particular function and U is some function of x and y. Furthermore, ψ_{sl} is normalized such that

$$\int_{-\ell/2}^{\ell/2} dx \int_{-w/2}^{w/2} dy\, \psi_{qr}^* \psi_{sl} = G_{\binom{q\ s}{r\ l}} \approx \delta_{s,q}\delta_{l,r} \equiv \delta_{\binom{q\ s}{r\ l}}. \tag{21}$$

For future conciseness, we define $N \equiv 1/(\epsilon\kappa_0^2 - \gamma^2)$ and

$$\mathcal{S}_s^{(\alpha)} \equiv \sin\left[\alpha_s\left(x-\frac{\ell}{2}\right)\right] \qquad \mathcal{S}_l^{(\beta)} \equiv \sin\left[\beta_l\left(y-\frac{w}{2}\right)\right]$$
$$\mathcal{C}_s^{(\alpha)} \equiv \cos\left[\alpha_s\left(x-\frac{\ell}{2}\right)\right] \qquad \mathcal{C}_l^{(\beta)} \equiv \cos\left[\beta_l\left(y-\frac{w}{2}\right)\right],$$

so that

$$\psi_{sl} = \mathcal{E}_{sl}\left(A\mathcal{S}_s^{(\alpha)} + B\mathcal{C}_s^{(\alpha)}\right)\left(C\mathcal{S}_l^{(\beta)} + D\mathcal{C}_l^{(\beta)}\right). \tag{23}$$

4.1 Polarization Schemes

As in the Floquet modes, there are also two polarizations: TM, where $H_z = 0$, and TE, where $E_z = 0$.

For TM polarization we have

$$H_z = 0 \tag{24}$$

and E_{zsl} is

$$E_{zsl}^{TM} = \mathcal{E}_{sl}\mathcal{G}_{sl}\left(\mathcal{S}_s^{(\alpha)} + B_s\mathcal{C}_s^{(\alpha)}\right)\left(\mathcal{S}_l^{(\beta)} + D_l\mathcal{C}_l^{(\beta)}\right)e^{\pm i\gamma_{sl}(z+h/2)}, \tag{25}$$

where $B_s = D_l = 0$ for a perfect conductor, and $B_s = -\alpha_s'\zeta_\ell$ and $D_l = -\beta_l'\zeta_w$ for the skin depth approximation, see Appendix A.

For TE polarization we have

$$E_z = 0 \tag{26}$$

and H_{zsl} is

$$H_{zsl}^{TE} = \mathcal{E}_{sl}\mathcal{G}_{sl}\left(A_s\mathcal{S}_s^{(\alpha)} + \mathcal{C}_s^{(\alpha)}\right)\left(C_l\mathcal{S}_l^{(\beta)} + \mathcal{C}_l^{(\beta)}\right)e^{\pm i\gamma_{sl}(z+h/2)}, \tag{27}$$

where $A_s = C_l = 0$ for a perfect conductor, and $A_s = \alpha_s'\zeta_\ell$ and $C_l = \beta_l'\zeta_w$ for the skin depth approximation.

4.2 Total Fields in the Cavity

As with the superstrate and substrate, we can now write the total z components of the electric and magnetic fields in the cavity as the sum of all the individual TM and TE modes. For the upward propagating modes we use $\mathcal{A}_{sl}$ and $\mathcal{D}_{sl}$ as the expansion coefficients, and we use $\mathcal{B}_{sl}$ and $\mathcal{F}_{sl}$ as the expansion coefficients for the downward propagating modes. That is,

$$H_z^{\text{cavity}} = \sum_{s,l} \mathcal{E}_{sl} \left(A_s \mathcal{S}_s^{(\alpha)} + \mathcal{C}_s^{(\alpha)} \right) \left(C_l \mathcal{S}_l^{(\beta)} + \mathcal{C}_l^{(\beta)} \right) \left[\mathcal{D}_{sl} e^{i\gamma_{sl}(z+h/2)} + \mathcal{F}_{sl} e^{-i\gamma_{sl}(z+h/2)} \right] \tag{28a}$$

$$E_z^{\text{cavity}} = \sum_{s,l} \mathcal{E}_{sl} \left(\mathcal{S}_s^{(\alpha)} + B_s \mathcal{C}_s^{(\alpha)} \right) \left(\mathcal{S}_l^{(\beta)} + D_l \mathcal{C}_l^{(\beta)} \right) \left[\mathcal{A}_{sl} e^{i\gamma_{sl}(z+h/2)} + \mathcal{B}_{sl} e^{-i\gamma_{sl}(z+h/2)} \right] \tag{28b}$$

Then, the transverse fields are given by

$$\vec{H}_t = N \left[i\epsilon\kappa_0 \hat{z} \times \nabla_t E_z \pm i\gamma \nabla_t H_z \right] \tag{29a}$$

$$\vec{E}_t = N \left[\pm i\gamma \nabla_t E_z - i\kappa_0 \hat{z} \times \nabla_t H_z \right], \tag{29b}$$

where the choice of sign is positive for upward propagating waves and negative for downward propagating waves.

5. APPLICATION OF BOUNDARY CONDITIONS

As discussed in Section 2.2, both the magnetic fields and electric displacements are continuous across interfaces of constant dielectric. To ensure continuity of fields across an interface it is sufficient to force continuity of *only two* electric or magnetic field components per polarization (i.e. H_z and E_x or E_z and H_z, etc.). Therefore, since the total fields are written as a linear combination of two polarization states, we force continuity of four field components.

Given our polarization, we choose H_x and H_y to remain continuous, and, to account for SIBC, we choose ϵE_x and ϵE_y as the second two. We apply the SIBC on these latter two fields once at the cavity-film boundary, and we apply the SDBC at the cavity floor.

5.1 $z = h/2$ Boundary

The top interface is given by $z = h/2$, $-\ell/2 \le x \le \ell/2$ and $-w/2 \le y \le w/2$. Here we ensure continuity of H_x and H_y across the cavity-superstrate interface. We equate the x components of the magnetic fields evaluated at $z = h/2$, multiply both sides by $\mathcal{E}_{qr}^* \left(\mathcal{S}_q^{(\alpha)} + B_q \mathcal{C}_q^{(\alpha)} \right)^* \left(D_r \mathcal{S}_r^{(\beta)} - \mathcal{C}_r^{(\beta)} \right)^*$ and integrate over $-\ell/2 \le x \le \ell/2$ and $-w/2 \le y \le w/2$. We evaluate the integrals in Appendix B and get:

$$\begin{aligned} &\sum_{m,n} \left(\sin\theta_{mn} I_{mn}^{TM} - \sqrt{\epsilon_a}\, \xi_{mn} \cos\theta_{mn} I_{mn}^{TE} \right) \mathcal{E}_{qr}^* \mathcal{K}_{\left(\begin{smallmatrix} q & m \\ r & n \end{smallmatrix}\right)} + \sum_{m,n} \left(\sin\theta_{mn} H_{mn}^{TM} + \sqrt{\epsilon_a}\, \xi_{mn} \cos\theta_{mn} E_{mn}^{TE} \right) \mathcal{E}_{qr}^* \mathcal{K}_{\left(\begin{smallmatrix} q & m \\ r & n \end{smallmatrix}\right)} \\ &\qquad = \sum_{s,l} i\epsilon_c \kappa_0 N_{sl} \beta_l G_{\left(\begin{smallmatrix} q & s \\ r & l \end{smallmatrix}\right)} \left[\mathcal{A}_{sl} e^{i\gamma_{sl} h} + \mathcal{B}_{sl} e^{-i\gamma_{sl} h} \right] - \sum_{s,l} i\gamma_{sl} N_{sl} \alpha_s G_{\left(\begin{smallmatrix} q & s \\ r & l \end{smallmatrix}\right)} \left[\mathcal{D}_{sl} e^{i\gamma_{sl} h} - \mathcal{F}_{sl} e^{-i\gamma_{sl} h} \right] \end{aligned} \tag{30}$$

Similarly, we equate the y components of the magnetic fields evaluated at $z = h/2$, multiply both sides by $\mathcal{E}_{qr}^* \left(A_q \mathcal{S}_q^{(\alpha)} + \mathcal{C}_q^{(\alpha)} \right)^* \left(\mathcal{S}_r^{(\beta)} - C_r \mathcal{C}_r^{(\beta)} \right)^*$ and integrate, giving

$$\begin{aligned} &\sum_{m,n} \left(-\cos\theta_{mn} I_{mn}^{TM} - \sqrt{\epsilon}_a\, \xi_{mn} \sin\theta_{mn} I_{mn}^{TE} \right) \mathcal{E}_{qr}^* \mathcal{L}_{\left(\begin{smallmatrix} q & m \\ r & n \end{smallmatrix}\right)} + \sum_{m,n} \left(-\cos\theta_{mn} H_{mn}^{TM} + \sqrt{\epsilon}_a\, \xi_{mn} \sin\theta_{mn} E_{mn}^{TE} \right) \mathcal{E}_{qr}^* \mathcal{L}_{\left(\begin{smallmatrix} q & m \\ r & n \end{smallmatrix}\right)} \\ &\qquad = \sum_{s,l} i\epsilon_c \kappa_0 N_{sl} \alpha_s G_{\left(\begin{smallmatrix} q & s \\ r & l \end{smallmatrix}\right)} \left[\mathcal{A}_{sl} e^{i\gamma_{sl} h} + \mathcal{B}_{sl} e^{-i\gamma_{sl} h} \right] - \sum_{s,l} i\gamma_{sl} N_{sl} \beta_l G_{\left(\begin{smallmatrix} q & s \\ r & l \end{smallmatrix}\right)} \left[\mathcal{D}_{sl} e^{i\gamma_{sl} h} - \mathcal{F}_{sl} e^{-i\gamma_{sl} h} \right] \end{aligned} \tag{31}$$

Now we ensure that

$$\epsilon_a E_x^{\text{super}} = -\epsilon_a \mathcal{Z} H_y^{\text{super}} \tag{32a}$$

$$\epsilon_a E_y^{\text{super}} = \epsilon_a \mathcal{Z} H_x^{\text{super}}. \tag{32b}$$

over the metallic region and ϵE_x and ϵE_y are continuous over the cavity. We evaluate these fields at $z = h/2$, multiply by $\exp\left[-i(k_{xg}x + k_{yf}y)\right]$ and integrate, piecewise, over the entire period.

We evaluate the integrals in Appendix B and get:

$$\begin{aligned}
&\epsilon_a \sum_{m,n} \left[-\left(\frac{1}{\sqrt{\epsilon_a}} \delta_{\binom{g\ m}{f\ n}} \xi_{mn} + \mathcal{Z}\mathcal{I}_{\binom{g\ m}{f\ n}} \right) \cos\theta_{mn} I_{mn}^{TM} + \left(\delta_{\binom{g\ m}{f\ n}} - \mathcal{Z}\sqrt{\epsilon_a}\, \mathcal{I}_{\binom{g\ m}{f\ n}} \xi_{mn} \right) \sin\theta_{mn} I_{mn}^{TE} \right] \\
&= \epsilon_a \sum_{m,n} \left[-\left(\frac{1}{\sqrt{\epsilon_a}} \delta_{\binom{g\ m}{f\ n}} \xi_{mn} - \mathcal{Z}\mathcal{I}_{\binom{g\ m}{f\ n}} \right) \cos\theta_{mn} H_{mn}^{TM} - \left(\delta_{\binom{g\ m}{f\ n}} + \mathcal{Z}\sqrt{\epsilon_a}\, \mathcal{I}_{\binom{g\ m}{f\ n}} \xi_{mn} \right) \sin\theta_{mn} E_{mn}^{TE} \right] \\
&+ \epsilon_c \sum_{s,l} i\gamma_{sl} N_{sl} \mathcal{E}_{sl} \alpha_s \mathcal{K}'_{\binom{g\ s}{f\ l}} \left[\mathcal{A}_{sl} e^{i\gamma_{sl}h} - \mathcal{B}_{sl} e^{-i\gamma_{sl}h} \right] + \epsilon_c \sum_{s,l} -i\kappa_0 N_{sl} \mathcal{E}_{sl} \beta_l \mathcal{L}'_{\binom{g\ s}{f\ l}} \left[\mathcal{D}_{sl} e^{i\gamma_{sl}h} + \mathcal{F}_{sl} e^{-i\gamma_{sl}h} \right]
\end{aligned} \tag{33}$$

$$\begin{aligned}
&\epsilon_a \sum_{m,n} \left[-\left(\frac{1}{\sqrt{\epsilon_a}} \delta_{\binom{g\ m}{f\ n}} \xi_{mn} - \mathcal{Z}\mathcal{I}_{\binom{g\ m}{f\ n}} \right) \sin\theta_{mn} I_{mn}^{TM} - \left(\delta_{\binom{g\ m}{f\ n}} + \mathcal{Z}\sqrt{\epsilon_a}\, \mathcal{I}_{\binom{g\ m}{f\ n}} \xi_{mn} \right) \cos\theta_{mn} I_{mn}^{TE} \right] \\
&= \epsilon_a \sum_{m,n} \left[-\left(\frac{1}{\sqrt{\epsilon_a}} \delta_{\binom{g\ m}{f\ n}} \xi_{mn} - \mathcal{Z}\mathcal{I}_{\binom{g\ m}{f\ n}} \right) \sin\theta_{mn} H_{mn}^{TM} + \left(\delta_{\binom{g\ m}{f\ n}} + \mathcal{Z}\sqrt{\epsilon_a}\, \xi_{mn} \mathcal{I}_{\binom{g\ m}{f\ n}} \right) \cos\theta_{mn} E_{mn}^{TE} \right] \\
&+ \epsilon_c \sum_{s,l} -i\gamma_{sl} N_{sl} \mathcal{E}_{sl} \beta_l \mathcal{K}''_{\binom{g\ s}{f\ l}} \left[\mathcal{A}_{sl} e^{i\gamma_{sl}h} - \mathcal{B}_{sl} e^{-i\gamma_{sl}h} \right] + \epsilon_c \sum_{s,l} -i\kappa_0 N_{sl} \mathcal{E}_{sl} \alpha_s \mathcal{L}''_{\binom{g\ s}{f\ l}} \left[\mathcal{D}_{sl} e^{i\gamma_{sl}h} + \mathcal{F}_{sl} e^{-i\gamma_{sl}h} \right]
\end{aligned} \tag{34}$$

5.2 Skin-depth approximation at cavity floor

Here, we apply the perfect electric boundary conditions (4) at $z = -h/2 - \delta$ over the cavity floor. We apply the condition on E_z, multiply by $\mathcal{E}_{qr}^* \left(A_q \mathcal{S}_q^{(\alpha)} + \mathcal{C}_q^{(\alpha)} \right)^* \left(C_l \mathcal{S}_r^{(\beta)} + \mathcal{C}_r^{(\beta)} \right)^*$ and integrate over the cavity floor. This gives

$$\sum_{s,l} G_{\binom{q\ s}{r\ l}} \left[\mathcal{A}_{sl} e^{-i\gamma_{sl}\delta} + \mathcal{B}_{sl} e^{i\gamma_{sl}\delta} \right] = 0 \tag{35}$$

The condition on H_z, when multiplied and integrated similarly yields

$$\sum_{s,l} G_{\binom{q\ s}{r\ l}} \left[\mathcal{D}_{sl} e^{-i\gamma_{sl}\delta} - \mathcal{F}_{sl} e^{i\gamma_{sl}\delta} \right] = 0 \tag{36}$$

6. CONSTRUCTING A COUPLING MATRIX

At this point, we'd like to construct a coupling matrix to link the unknown quantities with the known. We are looking for a matrix-vector equation of the form:

$$\mathcal{M}\vec{\Psi} = \vec{\Theta} \tag{37}$$

However, looking at the results of Section 5, we see that our known (and unknown) quantities are rank 2 tensors (matrices). In order to get an equation like Eq. 37, we change indices.

For the Floquet mode, both m and n run from $-N$ to N, for a total of $(2N+1)^2$ modes. We choose a new index $\tilde{m}$ which runs from 1 to $(2N+1)^2$, cycling over each n for every m. We similarly define $\tilde{g}$ for the indices g and h which run from $-G$ to G. For the cavity modes, both s and l run from 1 to S, for a total of S^2 modes. We choose a new index $\tilde{s}$ which runs from 1 to S^2, cycling over ever l for each s. We similarly define $\tilde{q}$ for the

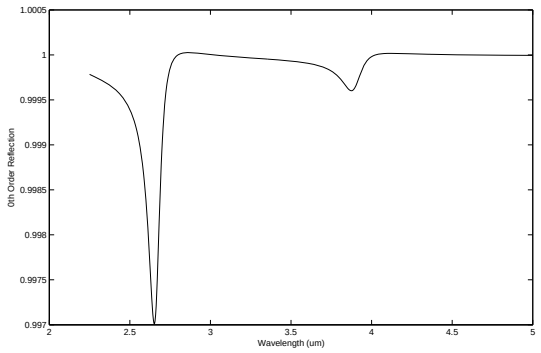

Figure 2. Results from preliminary code. 0th order (i.e. normal) TM reflection from a gold cavity, $\ell = 0.5\mu m$, $w = 1.75\mu m$, $h = 2\mu m$, and $\Lambda_x = \Lambda_y = 2\mu m$.

indices q and r which run from 1 to Q^2. Then, quantities like F_{mn} and G_{qr} become $F_{\tilde{m}}$ and $G_{\tilde{q}}$ and rank 4 tensor products like $\mathcal{F}_{\left(\begin{smallmatrix} q & m \\ r & n \end{smallmatrix}\right)}$ become rank 2 matrices $\mathcal{F}_{(\tilde{q}\tilde{m})} = \mathcal{F}_{\tilde{q}\tilde{m}}$.

Thus, in Eqs. (30), (31), (33), (34), (35), (36), any double-indexed (in the new notation) element can be viewed as a matrix, any single-indexed element can be viewed either as a vector or as a diagonal matrix, depending on the case. For example, the $\mathcal{A}_{\tilde{s}}$'s, etc., are turned into vectors while the $\xi_{\tilde{m}}$s, etc., are turned into diagonal matrices $\xi_{\tilde{m}\tilde{m}}$.

Thus, we can construct a coupling matrix $\mathcal{M}$ and vectors $\vec{\Psi}$ and $\vec{\Theta}$ as in Eq. 37.[12] Then, to find the unknown field components $\vec{\Psi}$, we simply invert each equation once:

$$\vec{\Psi} = \mathcal{M}^{-1}\vec{\Theta} \tag{38}$$

and then the solution for each set of initial conditions can be calculated by matrix multiplication. Fig. 2 shows some results from preliminary (incomplete) code. The plot shows 0th order (i.e. normal) TM reflection from TM incident fields. The dips in this reflection correspond to expected diffraction wavelengths, where some energy is reflected horizontally, decreasing the net transmission along the z direction.

7. CONCLUSIONS AND FUTURE WORK

In this paper we've outlined a powerful technique for modeling 2D periodic metamaterials. This method has significant advantages over finite element or finite difference time domain *simulations*. This method makes use of accurate, fast, and versatile *calculations*. Here, accuracy is limited by only by the precision of computer calculations, and runs extremely fast, even on standard computer workstations; the example in Fig. 2 finishes in a fraction of a second. Similar simulations take significantly longer (on the order of hours) to solve, especially at optical frequencies.

Furthermore, although the structure we've discussed here is a fairly simple single-cavity structure, it can be generalized to more complicated, compound structures. This analysis is needed for the multijunction analysis which has two (or more) cavity structures of different dimensions. This requires additional expansion coefficients for the added cavity modes, and integrals over the additional interface regions, but the fundamental analysis remains the same. Additionally, we are not limited to rectangular cavities; any structure with functional cavity modes (e.g. cylinders) can be similarly modeled.

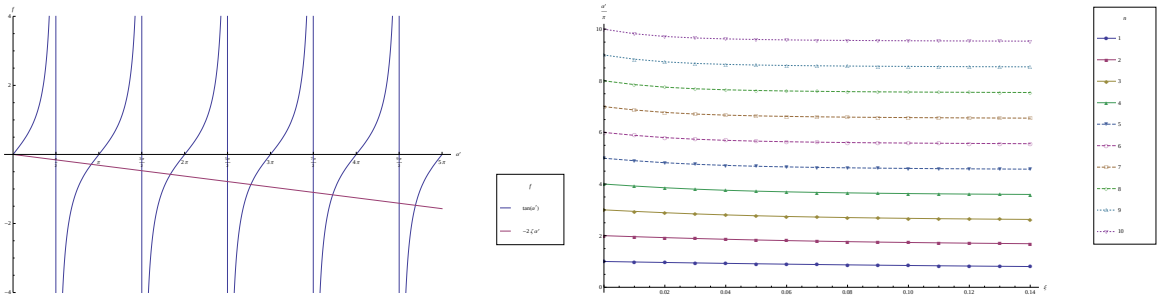

(a) Graphical depiction of Eq. 42. Points of intersection correspond to α's.

(b) Numerically solved values for α'/π plotted as a function of ζ. Each curve corresponds to a different root.

Figure 3. Graphical depiction and solutions of Eq. 42.

APPENDIX A. BOUNDARY CONDITIONS ON SOLUTIONS TO THE WAVE EQUATION

A.1 Perfect Conductor Boundary Condition

For a perfect conductor, we require

$$\psi^{TM}\big|_S = 0, \qquad \left.\frac{\partial \psi^{TE}}{\partial n}\right|_S = 0, \tag{39}$$

where $\partial/\partial n$ is a unit normal at the surface S.[10] These conditions give values for A and B or C and D as well as α and β. Application of these conditions on Eq. (20) gives

$$\alpha_s = \frac{s\pi}{\ell}, \qquad \beta_l = \frac{l\pi}{w}, \tag{40}$$

where s, l are integers and $B = D = 0$ for TM and $A = C = 0$ for TE modes.

A.2 Excellent Conductor - Skin Depth Approximation

In a nearly perfect conductor, the field does not stop immediately upon entering the metal. Instead, the magnitude of the fields decay exponentially with a characteristic length δ. As discussed in Section 2.2, we apply conditions Eqs. (39) at the skin depth, rather than at the metal surface. After simplification, these conditions yield

$$\alpha_s = \frac{\alpha'_s}{\ell}, \qquad \beta_l = \frac{\beta'_l}{w} \tag{41}$$

where α'_s and β'_l are the sth and lth roots of

$$\tan\alpha' = -2\alpha'\zeta_\ell, \qquad \tan\beta' = -2\beta'\zeta_w \tag{42}$$

respectively, where $\zeta_\ell = \delta/\ell$ and $\zeta_w = \delta/w$, and $B = -A\alpha'\zeta_\ell$ and $D = -C\beta'\zeta_w$ for TM and $A = B\alpha'\zeta_\ell$ and $C = D\beta'\zeta_w$ for TE. Eq. (42) is depicted graphically in Fig. 3(a) with numerically computed solutions in Fig. 3(b). These solutions can be fit with an arctangent function, allowing for quicker computation of these roots.

APPENDIX B. INTEGRALS

Here we integrate over the interface between the cavity and superstrate. We will make use of the following general integrals in our calculations:

$$J_{ij}^{\mu\nu}(a) \equiv \int_{-a/2}^{+a/2} d\tau\, e^{i\mu_i\tau}\sin[\nu_j(\tau - a/2)] = \begin{cases} \frac{e^{ia\mu_i/2}\left[\nu_j e^{ia\mu_i} - i\mu_i\sin(a\nu_j) - \nu_j\cos(a\nu_j)\right]}{\mu_i^2 - \nu_j^2} & \mu_i \neq \nu_j \\ \frac{e^{-3ia\mu_i/2}\left[1 + e^{2ia\mu_i}(-1 + 2ia\mu_i)\right]}{4\mu_i} & \mu_i = \nu_j \end{cases} \tag{43a}$$

and

$$K_{ij}^{\mu\nu}(a) \equiv \int_{-a/2}^{+a/2} d\tau\, e^{i\mu_i\tau}\cos[\nu_j(\tau - a/2)] = \begin{cases} \frac{ie^{-ia\mu_i/2}\left[\mu_i\cos(a\nu_j)+\mu_i\left(-e^{ia\mu_i}\right)+i\nu_j\sin(a\nu_j)\right]}{\mu_i^2-\nu_j^2} & \mu_i \neq \nu_j \\ \frac{e^{-3ia\mu_i/2}\left[e^{2ia\mu_i}(2a\mu_i-i)+i\right]}{4\mu_i} & \mu_i = \nu_j \end{cases}. \tag{43b}$$

Here μ stands in for k_x or k_y and i stands in for m or n (or g or f), respectively. Similarly, ν stands in for α or β and j stands in for s or l (or q or r), respectively. Likewise, a stands in for either ℓ or w. Additionally, the approximations noted in the equations represent that, in general, there is no inherent connection between μ_i (the wavevector in the superstrate) and ν_j (the wavevector in the substrate). Were $\mu_i = \nu_j$ these integrals would take a different form.

Then,

$$\mathcal{K}_{\left(\begin{smallmatrix} q & m \\ r & n \end{smallmatrix}\right)} = \left[J_{mq}^{k_x\alpha}(\ell) + B_q^* K_{mq}^{k_x\alpha}(\ell)\right]\left[D_r^* J_{nr}^{k_y\beta}(w) - K_{nr}^{k_y\beta}(w)\right] \tag{44a}$$

$$\mathcal{L}_{\left(\begin{smallmatrix} q & m \\ r & n \end{smallmatrix}\right)} = \left[A_q^* J_{mq}^{k_x\alpha}(\ell) + K_{mq}^{k_x\alpha}(\ell)\right]\left[J_{nr}^{k_y\beta}(w) - C_r^* K_{nr}^{k_y\beta}(w)\right] \tag{44b}$$

and

$$\mathcal{K}'_{\left(\begin{smallmatrix} s & g \\ l & f \end{smallmatrix}\right)} = \left[K_{gs}^{*k_x\alpha}(\ell) - B_s J_{gs}^{*k_x\alpha}(\ell)\right]\left[J_{fl}^{*k_y\beta}(w) + D_l K_{fl}^{*k_y\beta}(w)\right] \tag{44c}$$

$$\mathcal{L}'_{\left(\begin{smallmatrix} s & g \\ l & f \end{smallmatrix}\right)} = \left[A_s J_{gs}^{*k_x\alpha}(\ell) + K_{gs}^{*k_x\alpha}(\ell)\right]\left[C_l^* K_{fl}^{*k_y\beta}(w) - J_{fl}^{*k_y\beta}(w)\right] \tag{44d}$$

and

$$\mathcal{K}''_{\left(\begin{smallmatrix} s & g \\ l & f \end{smallmatrix}\right)} = \left[J_{mq}^{*k_x\alpha}(\ell) + B_q K_{mq}^{*k_x\alpha}(\ell)\right]\left[K_{fl}^{*k_y\beta}(w) - D_l J_{fl}^{*k_y\beta}(w)\right] \tag{44e}$$

$$\mathcal{L}''_{\left(\begin{smallmatrix} s & g \\ l & f \end{smallmatrix}\right)} = \left[A_s K_{gs}^{*k_x\alpha}(\ell) - J_{gs}^{*k_x\alpha}(\ell)+\right]\left[C_l J_{nr}^{*k_y\beta}(w) + K_{nr}^{*k_y\beta}(w)\right] \tag{44f}$$

And, for integrals over the metallic region,

$$\mathcal{I}_{\left(\begin{smallmatrix} g & m \\ f & n \end{smallmatrix}\right)} = \Lambda_x\Lambda_y\delta_{\left(\begin{smallmatrix} g & m \\ f & n \end{smallmatrix}\right)} - I^{xy}_{\left(\begin{smallmatrix} g & m \\ f & n \end{smallmatrix}\right)} \tag{45}$$

where $I^{xy}_{\left(\begin{smallmatrix} g & m \\ f & n \end{smallmatrix}\right)} \equiv I_{mg}^{x\ell} I_{nf}^{yw}$ and

$$I_{ij}^{a\mu} = \begin{cases} \frac{\Lambda_\mu}{\pi(i-j)}\sin\left[\frac{(i-j)a\pi}{\Lambda\mu}\right] & i \neq j \\ a & i = j \end{cases} \tag{46}$$

ACKNOWLEDGMENTS

This material is based upon work supported by the DOD/DARPA SBIR PROGRAM under Contract No. W31P4Q-10-C-0074. The views, opinions, and/or findings contained in this article/presentation are those of the author/presenter and should not be interpreted as representing the official views or policies, either expressed or implied, of the Defense Advanced Research Projects Agency or the Department of Defense.

REFERENCES

[1] Ebbesen, T. W., Lezec, H. J., Ghaemil, H. F., Thiol, T., and Wolff, P. A., "Extraordinary optical transmission through sub-wavelength hole arrays," *Nature* **391**, pp. 667–669, Feb. 1998.

[2] Bethe, H. A., "Theory of diffraction by small holes," *Phys. Rev.* **66**, pp. 163–182, Oct 1944.

[3] Gordon, R., "Bethe's aperture theory for arrays," *Phys. Rev. A* **76**, p. 053806, Nov 2007.

[4] Shelby, R. A., Smith, D. R., and Schultz, S., "Experimental verification of a negative index of refraction," *Science* **292**(5514), pp. 77–79, 2001.

[5] Zhou, D. and Biswas, R., "Photonic crystal enhanced light-trapping in thin film solar cells," *Journal of Applied Physics* **103**(9), p. 093102, 2008.

[6] Bayindir, M., Temelkuran, B., and Ozbay, E., "Photonic-crystal-based beam splitters," *Applied Physics Letters* **77**(24), pp. 3902–3904, 2000.

[7] Crouse, D., "Numerical modeling and electromagnetic resonant modes in complex grating structures and optoelectronic device applications," *IEEE Transactions on Electron Devices* **52**, pp. 2365 – 2373, Nov. 2005.

[8] Crouse, D., Hibbins, A. P., and Lockyear, M. J., "Tuning the polarization state of enhanced transmission in gratings," *Applied Physics Letters* **92**(19), p. 191105, 2008.

[9] Crouse, D. and Keshavareddy, P., "Polarization independent enhanced optical transmission in one-dimensional gratings and device applications," *Opt. Express* **15**(4), pp. 1415–1427, 2007.

[10] Jackson, J., *Classical Electrodynamics*, John Wiley & Sons, Inc., 2nd ed., 1975.

[11] Lochbihler, H. and Depine, R., "Highly conducting wire gratings in the resonance region," *Applied Optics* **32**, pp. 3459–3465, Feb. 1993.

[12] Lansey, E., Pishbin, N., and Crouse, D., "Rigorous coupled wave analysis of 2D periodic metamaterials." Unpublished, May 2010.